© 2015. Published by The Company of Biologists Ltd | The Journal of Experimental Biology (2015) 218, 2782-2792 doi:10.1242/jeb.125096

RESEARCH ARTICLE

Directional flow sensing by passively stable larvae

Heidi L. Fuchs[1,*], Adam J. Christman[1], Gregory P. Gerbi[2], Elias J. Hunter[1] and F. Javier Diez[3]

ABSTRACT

Mollusk larvae have a stable, velum-up orientation that may influence how they sense and react to hydrodynamic signals applied in different directions. Directional sensing abilities and responses could affect how a larva interacts with anisotropic fluid motions, including those in feeding currents and in boundary layers encountered during settlement. Oyster larvae (*Crassostrea virginica*) were exposed to simple shear in a Couette device and to solid-body rotation in a single rotating cylinder. Both devices were operated in two different orientations, one with the axis of rotation parallel to the gravity vector, and one with the axis perpendicular. Larvae and flow were observed simultaneously with near-infrared particle-image velocimetry, and behavior was quantified as a response to strain rate, vorticity and centripetal acceleration. Only flows rotating about a horizontal axis elicited the diving response observed previously for oyster larvae in turbulence. The results provide strong evidence that the turbulence-sensing mechanism relies on gravity-detecting organs (statocysts) rather than mechanosensors (cilia). Flow sensing with statocysts sets oyster larvae apart from zooplankters such as copepods and protists that use external mechanosensors in sensing spatial velocity gradients generated by prey or predators. Sensing flow-induced changes in orientation, rather than flow deformation, would enable more efficient control of vertical movements. Statocysts provide larvae with a mechanism of maintaining their upward swimming when rotated by vortices and initiating dives toward the seabed in response to the strong turbulence associated with adult habitats.

KEY WORDS: *Crassostrea virginica*, Mechanosensors, Shear, Statocysts, Veligers, Vorticity

INTRODUCTION

In the ocean, strong vertical gradients in chemical and physical properties make directed vertical motion ecologically important for planktonic organisms. Vertical motion is achieved partly through morphology that confers a passively stable body orientation: solid shells, spines or exoskeletons are asymmetric and more dense than seawater, creating an offset in the body's centers of buoyancy and gravity. This offset induces a gravitational torque that helps to maintain the body orientation relative to gravity and facilitates vertical swimming (Kessler, 1986). In turbulence or shear, however, the gravitational torque is counteracted by rotational velocity gradients (vorticity). Vorticity induces a viscous torque that rotates the organism, leading either to a change in the equilibrium orientation or to tumbling (Kessler, 1986). Disruption of the vertical orientation can prevent upward swimming or cause passively stable swimmers to become trapped in layers of strong shear (Jonsson et al., 1991; Durham et al., 2009). Neutral buoyancy and symmetry promote tumbling (Karp-Boss and Jumars, 1998; Guasto et al., 2012), whereas excess density and an asymmetric density distribution promote a more stable orientation that enables directed vertical swimming, even in organisms incapable of sensing gravity (Mogami et al., 2001; Grünbaum and Strathmann, 2003). Orientational stability may also enhance the ability of some organisms to sense hydrodynamic signals produced by physical processes or other organisms.

For zooplankton, sensitivity to hydrodynamic signals is affected by both body orientation and the flow-sensing mechanism. Hydrodynamic signals include deformations due to strain rate [e.g. $\gamma=0.5(\partial w/\partial x+\partial u/\partial z)$], rotational motion due to vorticity [e.g. $\xi=(\partial w/\partial x-\partial u/\partial z)$], and accelerations due to temporal changes in velocity (e.g. $\alpha=\partial u/\partial t$). Mechanical deformations could be sensed as bending or stretching of external mechanoreceptors, which include some copepod antennae, invertebrate larval cilia and protistan membrane receptors (Naitoh and Eckert, 1969; Mackie et al., 1976; Yen et al., 1992). Strains in any direction can induce a mechanical signal, although sensitivity varies with the signal orientation relative to the body and sensors (Fields, 2010). Vorticity-induced rotation and acceleration might be sensed with internal gravity receptors or accelerometers in the form of fluid-filled sacs containing one or more calcareous stones (statoliths) whose motion reaches sensory hair cells or receptors. Such organs include statocysts in mollusks, decapod crustaceans and some jellyfish, and statocyst-like organelles in some protists (reviewed by Budelmann, 1988). Statolith motion and a resulting signal may be induced by acceleration in any direction or by rotation about an axis with a horizontal component. Sensitivity to strains or accelerations may vary weakly with signal direction, whereas sensitivity to rotation implicitly depends on the signal direction relative to gravity.

Directional flow sensing may enhance survival in some ecological interactions. In turbulent environments, plankton size scales are comparable to the smallest (Kolmogorov) eddy scales; at these scales, turbulence is generally isotropic (statistically similar along each axis; e.g. Gargett et al., 1984; Antonia et al., 1994) and would not be a source of strongly directional signals. Zooplankton that avoid turbulent conditions may reduce encounters with predators and could do so by sensing the intensity of deformations, regardless of signal direction. However, flows can be more anisotropic in the feeding currents of planktivores and in boundary layers. Many planktivorous fish maintain a horizontal body posture and feed on zooplankton by generating suction currents that zooplankton could sense as acceleration or deformation along a mainly horizontal axis (e.g. Webb, 2002; Wainwright et al., 2007; Holzman et al., 2008). Flow near solid boundaries generates a strong velocity gradient normal to the substrate (e.g. $\partial u/\partial z$ near the bed) that settling larvae could sense as a vorticity-induced rotation (Nowell and Jumars, 1984; Jonsson et al., 1991; Mullineaux and Garland, 1993). An ability to distinguish the direction of hydrodynamic signals may enable zooplankton to

[1]Department of Marine and Coastal Sciences, Rutgers University, New Brunswick, NJ 08901, USA. [2]Physics Department, Skidmore College, Saratoga Springs, NY 12866, USA. [3]Mechanical and Aerospace Engineering, Rutgers University, New Brunswick, NJ 08901, USA.

*Author for correspondence (hfuchs@marine.rutgers.edu)

Received 13 May 2015; Accepted 27 June 2015

The Journal of Experimental Biology

The Journal of Experimental Biology (2015) 218, 2782-2792 doi:10.1242/jeb.125096

List of symbols

d	larval shell length
f	rotation frequency (Hz)
$\vec{F}_{v,N}$	noise floor of propulsive force estimates
$\vec{F}_v$	velar propulsive force vector
g	acceleration due to gravity
L	distance between centers of buoyancy and gravity
r	radial distance
Re	Reynolds number
r_i, r_o	inner and outer cylinder radii
u, w	horizontal and vertical fluid velocity
u_b, w_b	horizontal and vertical larval behavioral velocity
u_o, w_o	horizontal and vertical observed larval translational velocity
u_t	tangential velocity
w_T	larval terminal sinking velocity
ϕ	angle of vorticity-induced axial rotation relative to Cartesian axis
ν	kinematic viscosity (=0.01 $cm^2\ s^{-1}$)
ε	kinetic energy dissipation rate
η	Kolmogorov length scale
α	centripetal acceleration
γ	strain rate
θ_V	angle of larval propulsive force relative to larval axis
μ	dynamic viscosity
ξ	axial vorticity
ρ_p	larval density
ω	angular frequency

(All vertical velocities are positive in the upwards direction.)

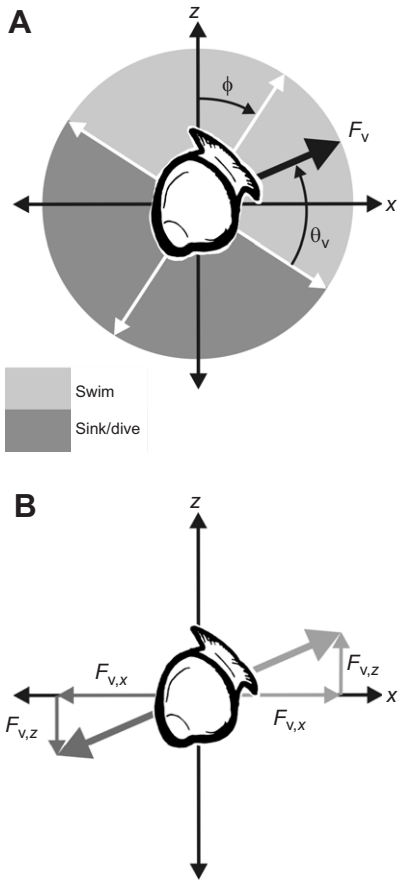

Fig. 1. Larval orientation diagram. (A) Axial rotation angle ϕ is measured relative to Cartesian axis (black), and propulsion angle θ_v is measured relative to larval axis (white) defined by the passively stable, velum-up larval orientation. Larvae are classified as swimming if propulsive force $\vec{F}_v$ is directed upward relative to the larval axis (light gray shaded region) and as sinking or diving if propulsive force is directed downward relative to the larval axis (dark gray shaded region). Redrawn from Fuchs et al. (2015). (B) Vector components of propulsive force depend on the axial rotation angle; at the rotation angle shown in A, the vertical component $\vec{F}_{v,z}$ is reduced and the horizontal component $\vec{F}_{v,x}$ is large.

avoid predators or enable larvae of benthic invertebrates to recognize the proximity of potential settlement sites.

Directional sensing may benefit larvae whose successful dispersal and settlement depend on an ability to move vertically through the water column. Larvae develop for weeks while being transported by currents that vary with depth, and upon becoming competent to metamorphose, larvae must migrate downward to settle on the seabed. During dispersal, depth-seeking behavior tends to limit transport and to enhance local retention (North et al., 2008; Shanks, 2009; Kim et al., 2010). Although larvae will contact substrates through diffusive processes alone, their supply to the bed can be greatly enhanced by sinking or swimming downward (Gross et al., 1992; Eckman et al., 1994; Fuchs et al., 2007). Transport to coastal habitats could also be enhanced by changes in vertical swimming or sinking behavior induced by turbulence (Barile et al., 1994; Welch and Forward, 2001; Fuchs et al., 2004, 2010). Larvae that respond to turbulence have stability-enhancing morphologies, but it is unclear whether larvae sense flow with directional specificity.

The present study focuses on whether signal direction affects flow sensing by oyster larvae (*Crassostrea virginica*). Oyster veligers have a dense, asymmetric larval shell that stabilizes the body orientation with the ciliated velum directed upward (Fig. 1). Oyster larvae respond to both turbulence and waves by either swimming faster upward or diving actively downward (Fuchs et al., 2013, 2015). In waves, these responses are elicited by high accelerations, indicating that statocysts can function as accelerometers (Fuchs et al., 2015). In turbulence, accelerations are generally smaller than those eliciting responses in waves, and larvae probably respond to strains or vorticity, both of which are highly correlated with the dissipation rate ε of turbulent kinetic energy (Tennekes and Lumley, 1972). Strains could be sensed as deformation of the velar cilia. These cilia are arranged on double bands around each velum and transect multiple planes, so sensitivity to strain should be multi-directional. Vorticity-induced rotation could be sensed by the statocysts, but sensitivity would depend on the axis of rotation. Thus, larvae have two potential turbulence-sensing mechanisms, only one of which would depend strongly on signal direction.

To tease apart the signal and mechanism enabling oyster larvae to sense turbulence, we did experiments in steady flows applied in two directions. Larvae were exposed to laminar shear in a Couette device and to solid-body rotation in a single cylinder (e.g. Kiørboe et al., 1999). Couette flow produces high strain rates and vorticity, whereas solid-body rotation produces negligible strain and constant vorticity. Rotating flows unavoidably produce centripetal acceleration, but here the accelerations were lower than those that previously induced larvae to dive in rectilinear wave motions (Fuchs et al., 2015). Each device was operated in two different orientations, one with its axis horizontal and one with its axis vertical (Figs 2,3). Strains produced about any rotational axis should deform the larval cilia, whereas only a horizontal component in the axis of rotation would affect larval orientation relative to gravity. An ability to sense these signals would be evidenced by larvae propelling themselves downward relative to the body axis; this diving behavior differs from swimming or passive sinking and has only been observed in

The Journal of Experimental Biology (2015) 218, 2782-2792 doi:10.1242/jeb.125096

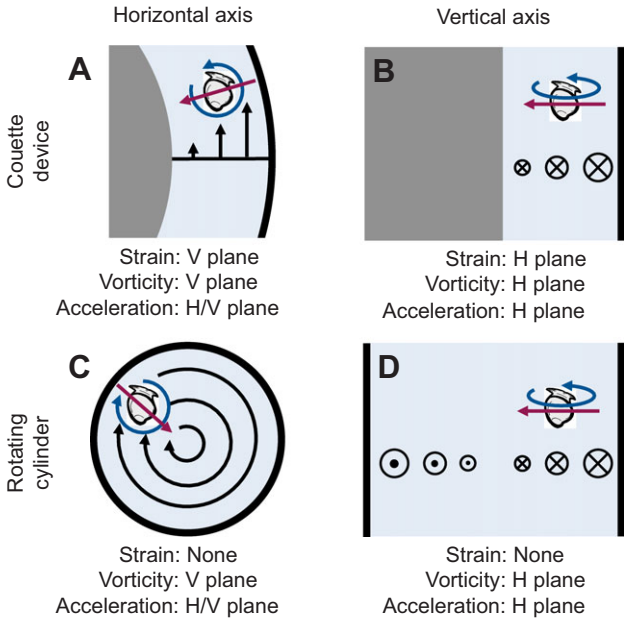

Fig. 2. Schematic of experimental conditions. (A,B) Couette device and (C,D) rotating cylinder with rotation about a horizontal (A,C) or vertical (B,D) axis. Black arrows and symbols indicate flow direction, red arrows indicate direction of centripetal acceleration, and blue arrows indicate whether larvae are rotated about their horizontal (circular arrows) or vertical (elliptical arrows) axes. Diagrams are not to scale. Strain rate γ, vorticity ξ, and centripetal acceleration α act on larvae in horizontal (H) or vertical (V) planes, as indicated below each diagram.

strong turbulence and large wave motions (Fuchs et al., 2013, 2015). The experimental design enabled us to pinpoint the turbulence-sensing mechanism (Table 1) to better understand the ecological significance of flow-mediated behavior.

RESULTS

Both the Couette device and rotating cylinder produced flows that were well predicted by theory at Reynolds number Re<2000

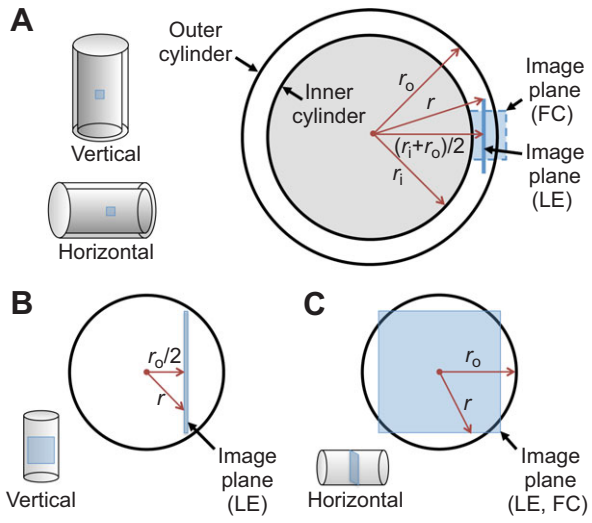

Fig. 3. Diagram of image plane locations. (A) Couette device and rotating cylinder in (B) vertical and (C) horizontal orientations. Image planes were centered along the length of the cylinders. Flow characterizations (FC) were done using the axial sections shown in (A,C) in both horizontal and vertical cylinder orientations. Larval experiments (LE) were done using lateral sections parallel to the long axis (A,B), except in the horizontally rotating cylinder (C).

(Tables 2,3). The Couette device produced laminar shear, except at the highest rotation frequency (Fig. 4), where there was some evidence of flow instability that resembled spiral turbulence (e.g. Andereck et al., 1986). Although Taylor (1923) considered this Couette configuration (stationary inner cylinder, rotating outer cylinder) to be universally stable, others have observed spiral turbulence at higher Reynolds numbers (Coles, 1965; Latz et al., 1994). The rotating flow performed as expected, but vorticity deviated slightly from theoretical values at the highest rotation rate (treatment R5, Table 3) about a horizontal axis (Fig. 5). At the highest rotation rate in both devices, the strain rate was more variable with rotation about a horizontal axis than about a vertical axis, probably reflecting orientational differences in the fluid's gravitational acceleration.

In behavior experiments, larvae dived only in flows rotating about a horizontal axis (Figs 6,7), ruling out strain rate as a potential signal for diving. In both devices, larvae were similar in size and density to larvae observed previously in unsteady flow (Table 4; Fuchs et al., 2013, 2015). We classified larvae as swimming or diving according to the direction of their propulsive force – upward or downward, respectively – relative to the larval axis, and we classified larvae as passively sinking if the downward propulsive force was weaker than the estimated noise level.

In the Couette device, swimming larvae showed no strong response to strain rate on either axis (Fig. 6C–F). With rotation about a horizontal axis, some larvae sank passively or dived at $\gamma \geq 0.4\ s^{-1}$ (corresponding to $\xi \geq 1\ s^{-1}$), but the percentage of larvae diving, the propulsive force used and the diving speed all reached maxima at intermediate rotation rates (Fig. 6A,C,E). At higher rotation rates, the reduced percentage of diving larvae may be an artifact of using a vertical image plane transecting a curved flow (Fig. 2A and Fig. 3A). At high rotation rates, the larvae would be rotated by vorticity, and their propulsive force would be directed away from the image plane. Larvae diving forcefully would have a large velocity component directed out of the image plane (Fig. 1B) and would be more difficult to observe at higher rotation rates. Thus the behavioral velocities and propulsive forces may have been underestimated for larvae diving at high strain rates.

In the rotating cylinder, larvae showed no response when rotated about a vertical axis, but changed both their swimming and diving behavior when rotated about a horizontal axis (Fig. 7). Over the tested range of horizontal vorticity, swimming larvae increased their propulsive force by a factor of 5 and transitioned from mostly negative (downward) to mostly positive (upward) vertical velocities (Fig. 7C,E). Sinking and diving were infrequent at low vorticity, but at $\xi \geq 4\ s^{-1}$ the percentage of diving larvae rose to a maximum of ~40% (Fig. 7A). Above this threshold, diving larvae consistently used as much or more propulsive force than swimming larvae (Fig. 7C). Diving velocities were more negative than the terminal fall velocity (Fig. 7E), but because the highest propulsive forces coincided with strong vorticity-induced larval rotation, larvae failed to reach the high diving speeds observed previously in turbulence ($w_b \approx 3 w_T$; Fuchs et al., 2013, 2015).

Combined data from the two devices showed very different responses to signals applied vertically versus horizontally. About a vertical axis (Fig. 8), swimming larvae showed a slight increase in propulsive force and swimming speed over the tested ranges of strain rate. However, we attribute this pattern to the inherent behavioral differences between larval batches used in the Couette device, where strain rate was high, and in the rotating cylinder, where strain rate was low. Larvae in vertical cylinders showed no response to the vertical component of vorticity. About a horizontal

The Journal of Experimental Biology (2015) 218, 2782-2792 doi:10.1242/jeb.125096

Table 1. Hypothetical responses to experimental conditions

Signal (sensor)		Dive response expected?			
		Couette device		Rotating cylinder	
Strains (cilia)	Vorticity-induced rotation (statocysts)	Horizontal axis	Vertical axis	Horizontal axis	Vertical axis
X		Yes	Yes	No	No
	X	Yes	No	Yes	No
X	X	Yes	Yes	Yes	No
		No	No	No	No

Each row indicates which experiments should produce a dive response, given the indicated signal(s) and sensor(s). Statocysts could also sense centripetal accelerations α, but in this study α was always below the threshold accelerations inducing frequent diving ($\sim 10^2$ cm s^{-2}; Fuchs et al., 2015).

axis (Fig. 9), larvae dived more frequently (Fig. 9A,B), and both swimming and diving larvae propelled themselves with greater force (Fig. 9E,F) at higher vorticity. Intuitively, the rise in propulsive force should produce a steady increase in swimming or diving speeds, but because the larval rotation angle also increased (Fig. 9C,D), there was no strong trend in larval vertical velocity (Fig. 1B and Fig. 9G,H).

Because axial vorticity and centripetal acceleration are correlated, there is a small possibility that larvae respond only to accelerations. However, the maximum centripetal accelerations α in this study were lower than the rectilinear accelerations that induced frequent diving previously (Fuchs et al., 2015). Moreover, centripetal acceleration magnitudes were independent of the axis of rotation, and the lack of response to flows about a vertical axis (Fig. 8B,D,F) suggests that acceleration alone was insufficient to induce a behavioral response.

DISCUSSION

All results point to vorticity-induced rotation about a horizontal axis as a primary stimulus eliciting the larval diving behavior. Larvae in this study experienced strain rates and vorticity within or above the ranges previously associated with a strong diving response in grid-stirred turbulence (Fuchs et al., 2013), yet these signals elicited a response only when rotation affected the larval orientation relative to gravity. There is strong evidence that larval statocysts function both as accelerometers (Fuchs et al., 2015) and as gravity detectors (Figs 9,10). The statocysts' dual sensing mechanism sets oyster larvae apart from plankton that sense spatial velocity gradients using external mechanoreceptors. Many copepods and ciliates sense mechanical deformations using antennae or membrane receptors, respectively (Naitoh and Eckert, 1969; Strickler and Bal, 1973; Yen et al., 1992; Echevarria et al., 2014), and they respond to strains with rapid jumps, which enable escape from predator-generated feeding currents (Kiørboe et al., 1999; Jakobsen, 2001). Some feeding currents generate both high strains and high accelerations (Higham et al., 2006; Holzman et al., 2008), yet few plankton react to accelerations (e.g. Heuch and Karlsen, 1997; Kiørboe et al., 1999). Oyster larvae may be able to detect predators by their accelerations, using statocysts instead of mechanosensory cilia. However, the high threshold acceleration and the lack of a response to strains suggest that oyster larvae sense flow mainly through changes in body orientation, and their responses would enhance control of vertical movements.

Passively stable, ciliated larvae generally propel themselves upward unless they are rotated by a viscous torque (Pennington and Strathmann, 1990; Jonsson et al., 1991; Young, 1995; Chan, 2012). In turbulence or shear flows, vorticity-induced rotation reduces the upward component of velocity and can convert upward propulsion to net downward motion (Fig. 1B; Grünbaum and Strathmann, 2003; Clay and Grünbaum, 2010). In still water, oyster larvae propel themselves with just enough force to offset gravitational acceleration and maintain a near-zero velocity (Fuchs et al., 2015), using their excess density as a natural tether that is likely to enhance feeding currents (e.g. Strathmann and Grunbaum, 2006; Kiørboe, 2011). This hovering behavior can be disrupted by turbulent eddies or vortices that tilt the larva, reducing the upward component of propulsive force and causing the larva to sink. However, larvae can maintain upward motion by swimming at a higher speed using more propulsive force (McDonald, 2012; Fuchs et al., 2013, 2015). This study demonstrates that oyster larvae swim more forcefully in response to rotation relative to gravity, which affects their vertical orientation, but not in response to rotation on a horizontal plane, which has no effect on vertical motion. It would be less efficient for larvae to adjust their swimming speed by sensing flow with cilia, which transect multiple planes, because they would be relatively insensitive to strain direction. The use of statocysts enables larvae to modify their swimming in response only to signals that disrupt their ability to move vertically.

The more dramatic reaction to turbulence is active diving; in unsteady flow, diving can produce behavioral velocities up to ~3 times more negative than the terminal fall velocity (Fuchs et al., 2013, 2015). In this study, diving larvae failed to reach the high diving speeds observed previously, because the downward-directed component of propulsive force was reduced by strong vorticity-induced rotation (Fig. 1B). In turbulence, however, rapid dives have clear benefits for enhancing settlement success. Oysters form discrete patches of reef that are rougher than surrounding soft

Table 2. Couette device experiment parameters

Treatment	f (s^{-1})	ω (rad s^{-1})	Re	$u_t(r)$ (cm s^{-1})	$\gamma(r)$ (s^{-1})	$\xi(r)$ (s^{-1})	$\alpha(r)$ (cm s^{-2})	Fps (pairs s^{-1})
C1	0.026	0.16	300	1.4	0.4	0.9	0.2	7.4
C2	0.041	0.26	470	2.2	0.6	1.4	0.6	7.4
C3	0.073	0.46	830	3.9	1.0	2.5	1.8	14
C4	0.15	0.91	1700	7.8	2.0	5.1	7.1	14
C5	0.26	1.6	2900	14	3.5	8.9	22	40

Includes treatment number, average frequency f, angular frequency ω, Reynolds number (Eqn 1), tangential velocity $u_t=r\omega$, strain rate γ (Eqn 2), axial vorticity ξ (Eqn 3), and centripetal acceleration α (Eqn 4) estimated at mid-gap [$r=(r_i+r_o)/2$], and image capture rate in frame pairs s^{-1}.

The Journal of Experimental Biology (2015) 218, 2782-2792 doi:10.1242/jeb.125096

Table 3. Rotating cylinder experiment parameters

Treatment	f (s^{-1})	ω (rad s^{-1})	Re	$u_t(r)$ (cm s^{-1})	$\xi(r)$ (s^{-1})	$\alpha(r)$ (cm s^{-2})	Fps (pairs s^{-1})
R1	0.087	0.54	290	1.2	1.0	0.6	7.4/7.4
R2	0.14	0.88	500	2.1	1.8	1.8	7.4/10
R3	0.25	1.6	890	3.7	3.1	5.9	10/14
R4	0.45	2.8	1600	6.7	5.7	19	10/30
R5	0.81	5.1	2900	12	10	60	14/40

Includes treatment number, average frequency f, angular frequency ω, rotational Reynolds number (Eqn 5), tangential velocity $u_t=r\omega$, axial vorticity ξ (Eqn 6) and centripetal acceleration α (Eqn 4) estimated at $r=r_o/2$, and image capture rate in frame pairs s^{-1} (horizontal/vertical).

substrates, raising local drag coefficients and dissipation rates (Whitman and Reidenbach, 2012; Styles, 2015). Although rough substrates can enhance settlement by providing refuges from turbulent stresses, they also enhance vertical mixing and increase the time it takes for some individual larvae to contact the bed (Eckman, 1990; McNair et al., 1997; Crimaldi et al., 2002; Reidenbach et al., 2009). Larvae that dive at high dissipation rates improve their chances of contacting a reef before they are swept past it and thus may settle at higher densities (Fuchs and Reidenbach, 2013). When larvae approach adult oysters on the substrate, settlement rates may be further enhanced by responses to chemical cues (Tamburri et al., 1992; Turner et al., 1994). Although turbulence could be sensed with either statocysts or mechanosensors, statocysts provide larvae with a single mechanism for controlling their upward swimming and initiating dives in response to the strong turbulence associated with adult habitats.

Oyster statocysts appear late in larval development and probably play an important sensory role only while larvae are competent to settle. In most bivalves, statocysts are present at the pediveliger stage (Carriker, 1990); in oysters, they form concurrently with the eyespots that are usually associated with onset of competency to metamorphose (Baker, 1994; Ellis and Kempf, 2011), and pre-competent larvae would be unable to sense flow. At settlement, larvae cement themselves to adult oysters or other solid substrates and become completely sessile (Prytherch, 1934; Kennedy and Sanford, 1999), rendering statocysts irrelevant. Because the larval shell maintains a stable orientation, Cragg and Nott (1977) hypothesized that the statocysts must be used for sensing substrate orientation while larvae crawl to explore settlement sites, but they did not consider the possibility of flow-induced larval rotation. Chia et al. (1981) later recognized that statocysts could also enable swimming larvae to detect turbulent water motion in nearshore habitats. The use of statocysts to detect fluid motion supports the idea that flow-induced larval behavior is adaptive in enhancing delivery to turbulent nearshore habitats prior to settlement.

Sensitivity to hydrodynamic signals probably increases with larval size as statoliths grow larger and more able to deform the sensory cells. Oyster statocysts are ~20 µm in diameter at the pediveliger stage (Ellis and Kempf, 2011). Within the statocyst, the Reynolds number is $Re \ll 1$, and statolith motion is governed by a balance of forces due to gravity, drag and a normal force exerted by the statocyst wall (Fig. 10). This balance is dominated by the gravitational force, which is proportional to the statolith radius cubed and thus increases exponentially as statoliths grow. Just as some larvae become less selective about settlement sites as they age (Knight-Jones, 1953; Marshall and Keough, 2003), oyster larvae may become more reactive to turbulence as they grow and gain a heightened sensitivity to vorticity.

Larvae in this study were slightly larger than those observed previously in turbulence and should have been more sensitive to rotation, yet they began diving at vorticities ~10 times higher than the previously estimated threshold ($\xi \approx 4$ versus 0.4 s^{-1}, Fig. 9; Fuchs et al., 2013). This result probably reflects a difference in how larval motion is affected by steady and unsteady flow. In intermittent turbulence, vorticity is unsteady, and the larval rotation angle would vary in time (Fig. 10C), whereas in the rotating flows used here, vorticity was steady, and the larval axial rotation angle would be at equilibrium (Fig. 10B). Assuming that larvae were

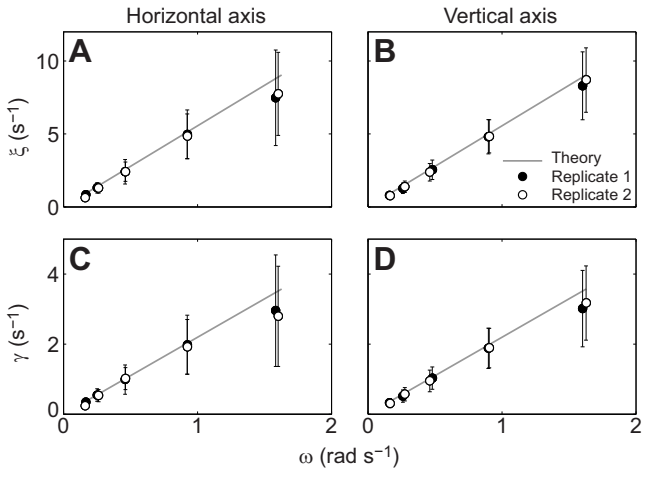

Fig. 4. Summary of hydrodynamic signals in the Couette device. (A,B) axial vorticity ξ and (C,D) strain rate γ versus angular frequency ω for rotation on horizontal (A,C) and vertical (B,D) axes. Symbols and error bars are means±1s.d. of values measured at mid-gap in replicated flow characterizations. Theoretical values are given by Eqns 2,3.

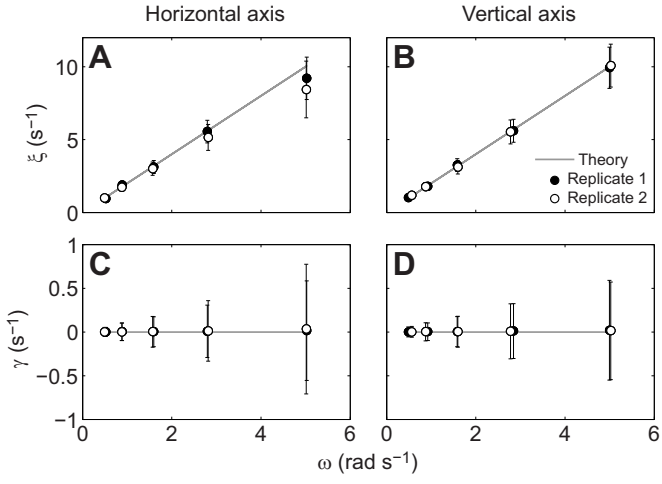

Fig. 5. Summary of hydrodynamic signals in the rotating cylinder. (A,B) axial vorticity ξ and (C,D) strain rate γ versus angular frequency ω for rotation on horizontal (A,C) and vertical (B,D) axes. Symbols and error bars are time- and space-averaged means±1s.d. of values measured in replicated flow characterizations. Theoretical values are $\xi=2\omega$ and $\gamma=0$.

The Journal of Experimental Biology (2015) 218, 2782-2792 doi:10.1242/jeb.125096

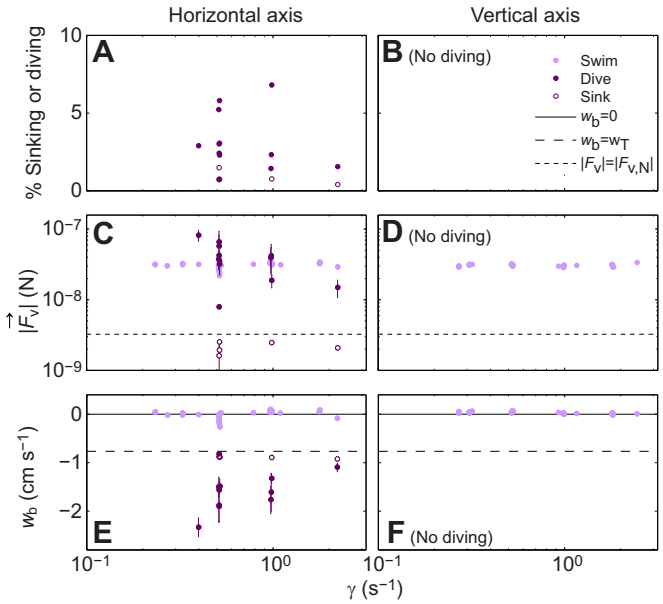

Fig. 6. Summary of larval behavior in Couette device. (A,B) Fraction of larvae sinking or diving, (C,D) propulsive force magnitude $|\vec{F}_V|$ and (E,F) vertical behavioral velocity w_b for larvae swimming, sinking passively or diving actively versus strain rate γ estimated indirectly from flow characterizations and larval radial positions. Symbols are averages of 100 instantaneous observations binned by strain rate for rotation about a horizontal (A,C,E) or vertical (B,D,F) axis, and error bars are ±1s.e. Some error bars are smaller than symbols. Dotted lines in C,D indicate noise floor $|\vec{F}_{V,N}|$ estimated for propulsive force magnitude of larvae sinking passively (Fuchs et al., 2015). Lines in E,F indicate neutral buoyancy (w_b=0, solid) and larval terminal fall velocity (w_b=w_T, dashed). No sinking or diving larvae were observed in the Couette device rotating about a vertical axis.

tilted steadily, the observed reactions were probably induced by continuous motion of the statoliths as larvae spun about their body axes while swimming in helices (e.g. Jonsson et al., 1991), which would create an 'apparent vorticity'. The apparent vorticity would be highest when larvae are rotated to ϕ=90 deg but would be limited by the time it takes for larvae to complete one helical revolution (~3–8 s). It is reasonable that larvae should be more sensitive to natural turbulence that produces motions on shorter time scales (≥0.01 s; H.L.F. and G.P.G., unpublished results).

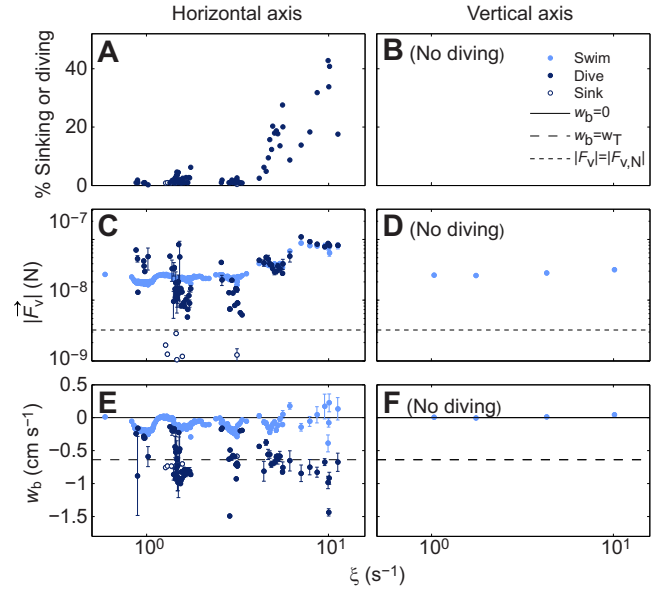

Fig. 7. Summary of larval behavior in rotating cylinder. Lines and symbols as in Fig. 6, plotted versus axial vorticity ξ measured directly (A,C,E) or estimated indirectly (B,D,F) from flow characterizations (one estimate per treatment). In vertical treatment R3 (Table 3), larvae could not be tracked because the frame rate was too low. No sinking or diving larvae were observed in the cylinder rotating about a vertical axis.

It remains unknown how statocysts are involved in behavioral signaling and control. Some nudibranch larvae have a neural connection between the statocysts and velar cilia via the central ganglia (Chia et al., 1981), and changes in orientation could signal a change in swimming speed or direction. The statocysts of oyster larvae have possible neural connections to the pedal and pleural ganglia (Ellis and Kempf, 2011), but the function of these connections is unknown. Holoplanktonic mollusks, including cephalopods and pteropods, experience higher Reynolds numbers than larvae and require greater maneuverability; accordingly, they have larger statocysts that are involved in complex neural signaling and even in the detection of sound (Budelmann, 1995; Levi et al., 2004; Mooney et al., 2010; Samson et al., 2014). Sound has also been proposed as a cue for oyster settlement (Lillis et al., 2013), but our flow devices produced the same sounds in both orientations, and the lack of response in vertical cylinders rules out sound as a behavioral cue in this study. Our results demonstrate that even small larval statocysts can function both as accelerometers and as gravity detectors. This dual functionality provides a mechanism for larvae to sense a wide range of hydrodynamic conditions and may enable larvae to distinguish vorticity-inducing turbulence from acceleration-inducing predators or waves (e.g. Denny, 1988; Koehl et al., 2013; H.L.F. and G.P.G., unpublished results).

Compared with plankton that use external mechanosensors, larvae that sense flow using statocysts may be more susceptible to disruption of sensory abilities by ocean acidification. Most molluskan statoliths are calcium carbonate (e.g. Hanlon et al., 1989; Zacherl et al., 2003) and can become degraded at the low saturation states resulting from elevated pCO_2 (e.g. Fabry et al., 2008; Kaplan et al., 2013). Statolith degradation would reduce statocyst functionality and could be especially problematic for larvae of estuarine species that use turbulence as a signal to initiate rapid descents in highly turbulent environments. Estuaries are naturally acidified as a result of the low buffering capacity of fresh water, short tidal time scales, and high community respiration rates (Wang and Cai, 2004; Cai, 2011). Although oysters are adapted to such conditions, both larvae and juveniles experience reduced shell growth at low pH or high pCO_2 (Calabrese and Davis, 1966; Miller et al., 2009; Waldbusser et al., 2011; Barton et al., 2012). Acidification-induced statolith degradation could potentially reduce larval sensitivity to turbulence, dampen the dive response and prevent larvae from achieving high settlement fluxes in energetic coastal habitats.

MATERIALS AND METHODS

Flow tanks

Couette flow

We tested larval responses to strains in a Couette device consisting of an outer cylinder rotating around a stationary inner cylinder. Couette flow is laminar at Reynolds numbers of Re<2000 to 4000 (Taylor, 1936; Coles, 1965; Latz et al., 1994; Warnaars and Hondzo, 2006), where Reynolds number is defined as

$$Re = \frac{\omega r_o (r_o - r_i)}{\nu}. \quad (1)$$

Here ω=2πf is the angular frequency in rad s^{-1}, f is frequency in Hz, r_o is the radius of the outer cylinder, r_i is the radius of the inner cylinder and ν=0.01 cm^2 s^{-1} is the kinematic viscosity. Another criterion for maintaining

The Journal of Experimental Biology (2015) 218, 2782-2792 doi:10.1242/jeb.125096

Table 4. Summary of *C. virginica* larval measurements

Tank	Replicate	d (μm)	w_T (cm s^{-1})	ρ_p (g cm^{-3})	N_T	N_O
Couette device	V1	310 [±12]	−0.72 [±0.11]	1.17	860	3114
	V2	307 [±11]	−0.77 [±0.09]	1.19	894	3202
	H1	311 [±13]	−0.77 [±0.08]	1.18	382	1620
	H2	309 [±10]	−0.81 [±0.07]	1.20	802	2607
Rotating cylinder	V1	319 [±11]	−0.62 [±0.08]	1.16	588	3171
	H1	317 [±9]	−0.64 [±0.08]	1.16	875	5230
	H2	314 [±11]	−0.65 [±0.08]	1.17	3700	27,102

Shell length d and terminal sinking velocity w_T are given as mean±1s.d. Larval densities ρ_p are single estimates calculated from mean shell length and terminal velocity. Rotation about vertical or horizontal axis is indicated by V and H preceding replicate number. Also included are number of trajectories N_T and number of instantaneous observations N_O in each replicate.

flow stability is that the gap should be narrow relative to the outer cylinder radius, $r_i/r_o \geq 0.8$ (e.g. Latz et al., 1994). In this study, the gap had to be large enough to enable unrestricted movement of veliger larvae, which swim in helices of several body lengths in diameter (e.g. Jonsson et al., 1991; Gallager, 1993). We used cylinder radii of r_i=7.6 cm and r_o=9.5 cm, giving r_i/r_o=0.8 with a gap width of 1.9 cm, or ∼63 larval body lengths. The rotation frequencies and Reynolds numbers were limited by the minimum motor speed and by our ability to track individual larvae (Table 2).

In the Couette device, the strain rate, vorticity in the axial direction and centripetal acceleration are defined as:

$$\gamma = \frac{\omega r_o^2 r_i^2}{r^2(r_o^2 - r_i^2)}, \quad (2)$$

$$\xi = \frac{2\omega r_o^2}{r_o^2 - r_i^2}, \quad (3)$$

$$\alpha = r\omega^2 = \frac{u_t^2}{r}, \quad (4)$$

where r is radial distance and $u_t(r)=r\omega$ is the tangential velocity (Kiørboe et al., 1999). In this experiment, centripetal accelerations α were lower than those inducing a response in unidirectional, oscillating flow (Fuchs et al., 2015), but strain rate γ and vorticity ξ were always within or above the ranges associated with a strong diving response by oyster larvae in grid-stirred turbulence (Table 2; Fuchs et al., 2013). If larvae react to strains using the cilia, sensitivity should be independent of flow direction, and larvae should exhibit a dive response in Couette flow regardless of the axis of rotation (Fig. 2 and Table 1).

Solid-body rotation

We tested larval responses to vorticity using a single rotating cylinder with radius r_o=4.8 cm. At steady state, the fluid in the cylinder rotates as a solid body (Tooby et al., 1977; Jackson, 1994; Kiørboe et al., 1999), and the rotational Reynolds number is:

$$Re = \frac{r_o^2 \omega}{4\nu}. \quad (5)$$

As in the Couette device, the rotation frequencies and Reynolds numbers were limited by minimum motor speed and larval tracking ability (Table 3).

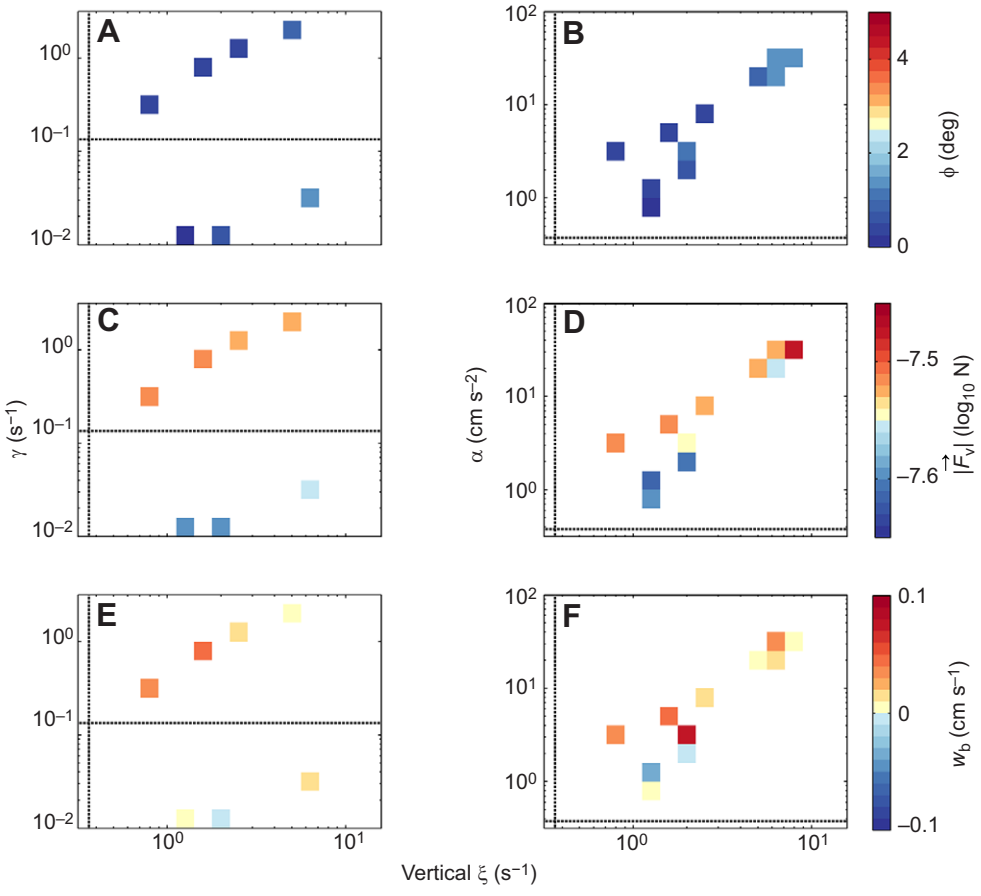

Fig. 8. Summary of swimming behavior in flows rotating about a vertical axis. (A,B) Larval axial rotation angle, (C,D) propulsive force magnitude and (E,F) behavioral vertical velocity. Instantaneous observations from Couette device and rotating cylinder are combined and averaged over small bins of strain rate (A,C,E) or acceleration (B,D,F) and the vertical component of vorticity. Rotation angles (A,B) are estimated from measured horizontal vorticity. Dashed lines represent estimated threshold values above which larvae dove frequently in isotropic turbulence (Fuchs et al., 2013). No diving larvae were observed.

The Journal of Experimental Biology (2015) 218, 2782-2792 doi:10.1242/jeb.125096

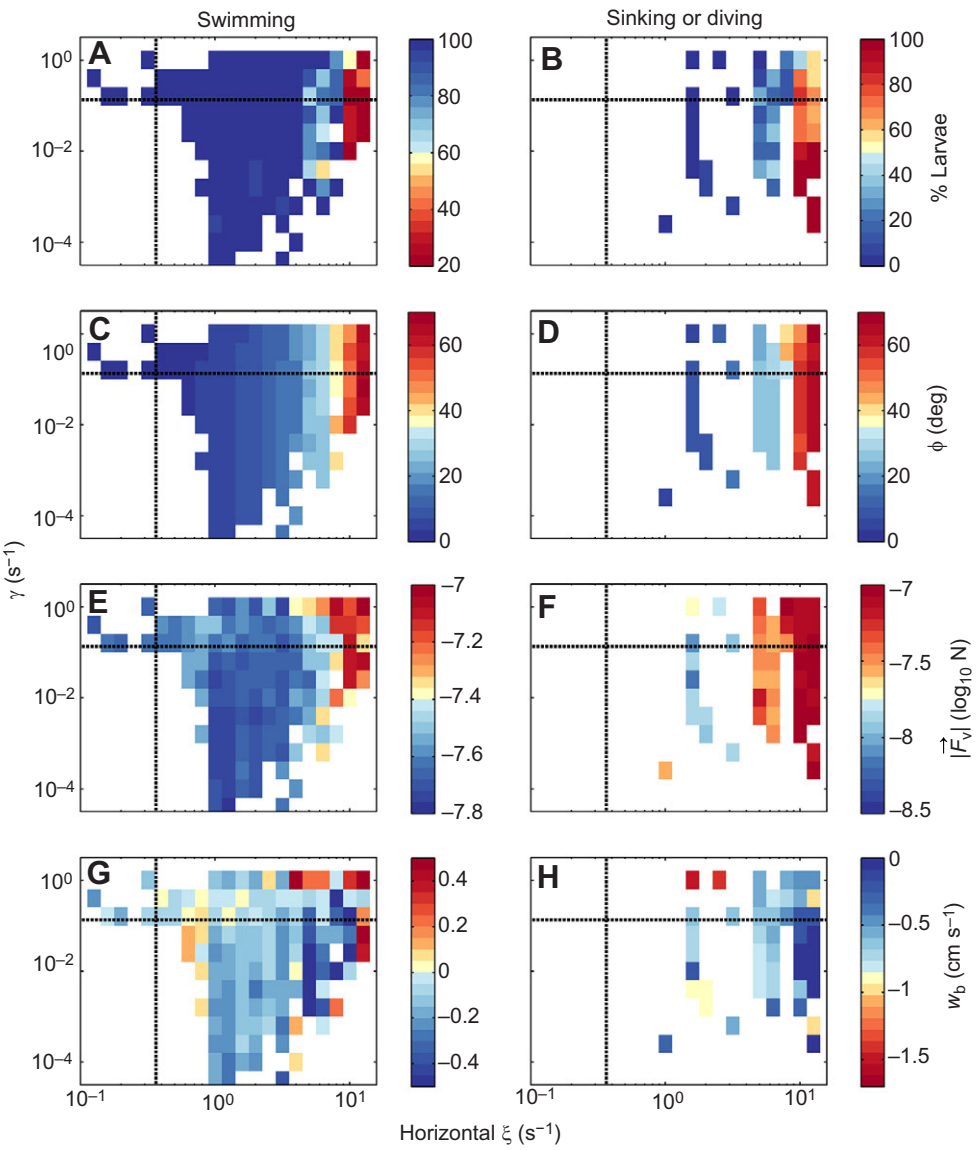

Fig. 9. Summary of larval behavior in flows rotating about a horizontal axis. (A,B) Percentage of larvae swimming or diving, (C,D) larval axial rotation angle, (E,F) propulsive force magnitude and (G,H) behavioral vertical velocity. Instantaneous observations from the Couette device and rotating cylinder are combined and averaged over small bins of strain rate and the horizontal component of vorticity. Dashed lines represent threshold values of strain or vorticity above which larvae dived frequently in isotropic turbulence (Fuchs et al., 2013). Bins with ≤1% swimming or diving larvae are omitted for clarity. Some colorbars differ on left and right.

For a single rotating cylinder, the vorticity in the axial direction is defined as:

$$\xi = 2\omega, \tag{6}$$

and the centripetal acceleration α is given by Eqn 4. The centripetal accelerations α were below those that induced a response in unidirectional, oscillating flow (Fuchs et al., 2015). The strain rate is theoretically zero at steady state, but the shear produced by initial rotation from rest can persist for long periods of time (Jackson, 1994). Here the average measured strain rates γ were typically one to two orders of magnitude lower than in the Couette experiments. In contrast, ξ was within or above the ranges associated with a dive response in turbulence (Fuchs et al., 2013). If larvae sense vorticity-induced rotation using the statocysts, sensitivity should depend on the axis of rotation, and the larvae should exhibit a dive response only in cylinders rotating about a horizontal axis (Fig. 2 and Table 1).

Flow characterization

For each device, we compared the flow to theoretical predictions by characterizing the 2-dimensional (2D) velocities at the cylinder mid-point in a plane normal to the cylinder axis. Velocities were measured using a planar particle-image velocimetry (PIV) system with a 4 megapixel CCD camera (FlowSense, Dantec Dynamics), a 100 mm lens (Tokina) and a DualPower pulsed green laser (532 nm Nd:YAG). For each device, five flow treatments were applied in a random order, with 10 min of no motion between treatments followed by a ≥10 min spin-up time and 2 min of recording at 7.4 frame pairs s^{-1}. In the Couette device, observations were made in an image plane spanning the gap between cylinders, observed at an angle from the side using a Scheimpflug mount (Fig. 3A). In the rotating cylinder, observations were made in an image plane transecting the cylinder (Fig. 3C). To reduce distortion of the laser sheet passing through the cylinders, each flow device was enclosed in an outer box filled with water (Wereley and Lueptow, 1999). All flow measurements were done twice in each device operating either horizontally or vertically.

Velocity vectors were computed using adaptive correlation algorithms in DynamicStudio software (Dantec). For these steady flows, we used interrogation areas of 64×64 or 128×128 pixels and 50% overlap to give vector resolutions of Δx=0.14 cm in the Couette device and Δx=0.23 cm in the rotating cylinder. Strain rate, vorticity and centripetal acceleration were calculated from measured velocities and their across-axis gradients; for example:

$$\gamma = \frac{1}{2}\left(\frac{\partial u}{\partial z} + \frac{\partial w}{\partial x}\right), \tag{7}$$

$$\xi = \frac{\partial w}{\partial x} - \frac{\partial u}{\partial z}, \tag{8}$$

$$\alpha = \frac{u^2 + w^2}{(x^2 + z^2)^{0.5}}, \tag{9}$$

The Journal of Experimental Biology (2015) 218, 2782-2792 doi:10.1242/jeb.125096

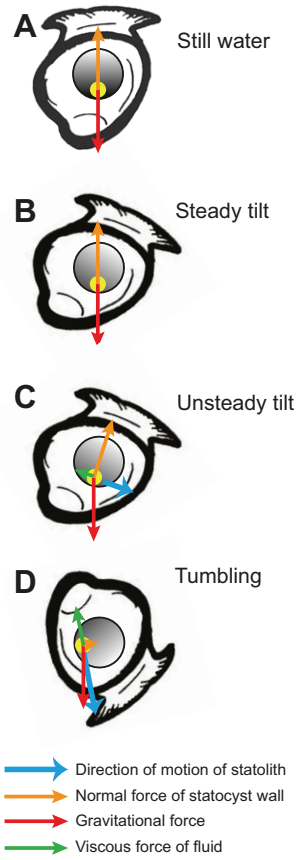

Fig. 10. Summary of forces on statolith. When the larva is in still water (A) or at a steady tilt (B), the statolith (yellow circle) is at rest within the statocyst (gray shaded circle) and experiences only the gravitational force and a normal force exerted by the statocyst wall. When the larva is at an unsteady tilt (C) or tumbling (D), the statolith rolls and experiences an added drag force. Note that even when the larval rotation angle is at equilibrium (B), the larva's helical swimming motion will spin the statocyst around the larval axis and induce the statolith to roll (not shown). Only one statocyst of a pair is shown, and drawing is not to scale; for anatomically correct scaling, see Ellis and Kempf (2011).

for cylinders in a horizontal orientation, where u and w are horizontal and vertical velocities, respectively.

Larval experiments

Eyed oyster larvae (*Crassostrea virginica* Gmelin 1791) were shipped overnight from Horn Point Laboratory (Maryland, USA) and used within 3 days. Most of these larvae were pediveligers. Different batches of larvae were used in each device: experiments were done in Couette flow 24–26 July 2013 and in the rotating cylinder 22–24 May 2013. Larvae were kept in 10 liter buckets of filtered seawater, aerated and fed *Isochrysis galbana* (T-Iso, 10^5 cells ml^{-1}) at 20°C. Experiments were done at 20.5°C. A salinity of 10 S_P (practical salinity) was used to match conditions at which larvae were reared.

The general experimental design, observational, and analytical approaches followed those described previously (Fuchs et al., 2013, 2015). Larvae and algae were added at concentrations of ~1 larva ml^{-1} and ~10^5 cells ml^{-1}, respectively, and gently mixed. After ~30 min in still water, larvae were observed in five flow treatments in random order with 10 min recovery times between treatments. Each treatment included a ≥10 min spin-up followed by 5 min of observations, except in three rotating treatments where observations began at the onset of rotation. In those treatments, initial observations were used to compare flows to the theoretical spin-up, but were excluded from analysis of larval motions. In the Couette device, experiments were replicated (N=2) in each orientation. In the rotating cylinder, experiments were replicated in the horizontal orientation and done once in the vertical orientation.

Larval behavior and flow were observed simultaneously using the PIV system with a near-infrared, pulsed diode laser (NanoPower 3 W, 808 nm). The infrared laser and natural algal seeding particles (~18 µm diatoms, *Thalassiosira weissflogii*, Reed Mariculture) were used to avoid larval behavioral artifacts caused by visible light and artificial particles (Fuchs et al., 2013). For observations in the Couette device, the IR laser was too weak to image flow across the gap between cylinders; instead, we used a 3.2-cm-wide, lateral image plane centered at the midpoint of the gap (Fig. 3A). In the rotating cylinder, the image plane was 7.5 cm wide in the lateral plane for the vertical orientation and in the axial plane for the horizontal orientation (Fig. 3B,C). All image planes were selected to resolve movements of larvae that respond to hydrodynamic signals mainly by changing their vertical motions.

At the end of each replicate, larvae were preserved in ethanol for measurement of shell length d and terminal sinking speed w_T. Shell length was measured digitally under a dissecting microscope (N=50 per replicate), and terminal sinking velocity was calculated from digital video of larvae sinking through a 2 liter settling column (N=83–964 per replicate) (Fuchs et al., 2013). Terminal sinking speeds were used to estimate larval density ρ_p from Rubey's modification of Stokes law, which accounts for inertia and is more accurate for particles in the larval size range (Rubey, 1933; Fuchs et al., 2013).

Behavior analysis

Larvae and flow often move in different directions, so PIV data from the behavior experiments were analyzed using approaches for two-phase flow (e.g. Kiger and Pan, 2000; Khalitov and Longmire, 2002; Cheng et al., 2010). Images were pre-processed to separate images of seeding particles and of larvae, which were used to calculate velocities of fluid flow and larvae, respectively (Fuchs et al., 2015). Flow velocities were computed from the particle images as described above for the flow characterizations. Larval translational velocities were estimated from larval trajectories constructed by particle tracking in Matlab. Fluid velocities were interpolated in time to match the larval observations using 3D, linear interpolation and then interpolated in space to larval locations using 2D, linear interpolation. The larval behavioral velocities, i.e. relative to the flow, were calculated from the instantaneous observed velocities of larvae and flow at their locations; for example, in the vertical direction $w_b=w_o-w$, where w_b is the velocity due to behavior, w_o is the observed translational velocity, and w is the fluid velocity. Horizontal velocities u and v were calculated similarly.

Two approaches were used to relate larval behavior to instantaneous hydrodynamic signals. For observations in the horizontally rotating cylinder (Fig. 3C), we estimated strain rate, vorticity and centripetal acceleration directly from gradients of velocity interpolated to the time and location of each larval observation. For all other observations in lateral planes (Fig. 3A,B), the hydrodynamic signals were primarily out of plane and could not be measured directly. Instead, we used the flow characterizations to estimate out-of-plane flow velocities and their gradients at the larval locations. Measured vorticity, strain rate and centripetal acceleration were interpolated to the larval radial location r and cylinder rotation frequency f using 2D, linear interpolation.

Behavior was analyzed as in previous studies to calculate the direction and magnitude of larval propulsive forces (Fuchs et al., 2013, 2015). The propulsive force vector $\vec{F}_v$ was calculated by solving a force balance equation that accounts for larval mass and acceleration, acceleration reaction force, net forces due to gravity and buoyancy, Stokes (viscous) drag and form (inertial) drag, Basset history force and force due to pressure gradients in the flow (e.g. Maxey and Riley, 1983; Mei et al., 1991). For details, see Appendix in Fuchs et al. (2015). We also estimated the angle of vorticity-induced axial rotation as:

$$\sin\phi = \frac{3\mu\xi}{L\rho_p g}, \qquad (10)$$

where µ is the dynamic viscosity, L≈3 µm is the distance between the centers of buoyancy and gravity, ρ_p is the larval density and g is the acceleration due to gravity (Kessler, 1986; Jonsson et al., 1991). Estimates

of ϕ were used to correct the Cartesian direction of larval propulsion to θ_v, the direction of propulsion relative to the larval axis as defined by the passively stable orientation (Fig. 1A; Fuchs et al., 2013). Larvae with propulsive force directed upward or downward relative to the larval axis were classified as swimming or diving, respectively, except that larvae were classified as passively sinking if the propulsive force was below the average noise floor of propulsive force estimates ($\vec{F}_{v,N} = 3.2 \times 10^{-9}$ N; Fuchs et al., 2015).

Acknowledgements
We thank D. Merritt and S. Alexander at Horn Point Laboratory for providing oyster larvae. E. Pirl assisted with larval cultures and measured the larval sizes and terminal fall velocities. The flow devices were designed by Epic Technologies and constructed by Diversified Designs. J. Grassle, and two anonymous reviewers provided helpful comments on the manuscript.

Competing interests
The authors declare no competing or financial interests.

Author contributions
H.L.F., G.P.G., and F.J.D. conceived and designed the research, A.J.C. did the flow characterizations, A.J.C. and H.L.F. performed the larval experiments, E.J.H. did the two-phase image separation, and H.L.F. analyzed the data and wrote the paper with a figure contributed by G.P.G.

Funding
Funding was provided by the National Science Foundation (OCE-1060622 to H.L.F., G.P.G. and F.J.D.).

References
Andereck, C. D., Liu, S. S. and Swinney, H. L. (1986). Flow regimes in a circular Couette system with independently rotating cylinders. *J. Fluid Mech.* **164**, 155-183.
Antonia, R. A., Zhu, Y. and Kim, J. (1994). Corrections for spatial velocity derivatives in a turbulent shear flow. *Exp. Fluids* **16**, 411-413.
Baker, P. (1994). Competency to settle in oyster larvae, *Crassostrea virginica*: wild versus hatchery-reared larvae. *Aquaculture* **122**, 161-169.
Barile, P. J., Stoner, A. W. and Young, C. M. (1994). Phototaxis and vertical migration of the queen conch (*Strombus gigas* linne) veliger larvae. *J. Exp. Mar. Biol. Ecol.* **183**, 147-162.
Barton, A., Hales, B., Waldbusser, G. G., Langdon, C. and Feely, R. A. (2012). The Pacific oyster, *Crassostrea gigas*, shows negative correlation to naturally elevated carbon dioxide levels: implications for near-term ocean acidification effects. *Limnol. Oceanogr.* **57**, 698-710.
Budelmann, B. U. (1988). Morphological diversity of equilibrium receptor systems in aquatic invertebrates. In *Sensory Biology of Aquatic Animals* (ed. J. Atema, R. R. Fay, A. N. Popper and W. N. Tavolga), pp. 757-782. New York: Springer-Verlag.
Budelmann, B. U. (1995). Cephalopod sense organs, nerves and the brain: adaptations for high performance and life style. *Mar. Fresh. Behav. Physiol.* **25**, 13-33.
Cai, W.-J. (2011). Estuarine and coastal ocean carbon paradox: CO_2 sinks or sites of terrestrial carbon incineration? *Annu. Rev. Mar. Sci.* **3**, 123-145.
Calabrese, A. and Davis, H. C. (1966). The pH tolerance of embryos and larvae of *Mercenaria mercenaria* and *Crassostrea virginica*. *Biol. Bull.* **131**, 427-436.
Carriker, M. R. (1990). Functional significance of the pediveliger in bivalve development. In *The Bivalvia – Proceedings of a Memorial Symposium in Honour of Sir Charles Maurice Yonge, Edinburgh 1986* (ed. B. Morton). Hong Kong: Hong Kong University Press.
Chan, K. Y. K. (2012). Biomechanics of larval morphology affect swimming: insights from the sand dollars *Dendraster excentricus*. *Integr. Comp. Biol.* **52**, 458-469.
Cheng, Y., Pothos, S. and Diez, F. J. (2010). Phase discrimination method for simultaneous two-phase separation in time-resolved stereo PIV measurements. *Exp. Fluids* **49**, 1375-1391.
Chia, F. S., Koss, R. and Bickell, L. R. (1981). Fine structural study of the statocysts in the veliger larva of the nudibranch, *Rostanga pulchra*. *Cell Tissue Res.* **214**, 67-80.
Clay, T. W. and Grünbaum, D. (2010). Morphology-flow interactions lead to stage-selective vertical transport of larval sand dollars in shear flow. *J. Exp. Biol.* **213**, 1281-1292.
Coles, D. (1965). Transition in circular Couette flow. *J. Fluid Mech.* **21**, 385-425.
Cragg, S. M. and Nott, J. A. (1977). The ultrastructure of the statocysts in the pediveliger larvae of *Pecten maximus* (L.) (Bivalvia). *J. Exp. Mar. Biol. Ecol.* **27**, 23-36.
Crimaldi, J. P., Thompson, J. K., Rosman, J. H., Lowe, R. J. and Koseff, J. R. (2002). Hydrodynamics of larval settlement: the influence of turbulent stress events at potential recruitment sites. *Limnol. Oceanogr.* **47**, 1137-1151.
Denny, M. W. (1988). *Biology and the Mechanics of the Wave-Swept Environment*. Princeton, NJ: Princeton University Press.
Durham, W. M., Kessler, J. O. and Stocker, R. (2009). Disruption of vertical motility by shear triggers formation of thin phytoplankton layers. *Science* **323**, 1067-1070.
Echevarria, M. L., Wolfe, G. V., Strom, S. L. and Taylor, A. R. (2014). Connecting alveolate cell biology with trophic ecology in the marine plankton using the ciliate *Favella* as a model. *FEMS Microbiol. Ecol.* **90**, 18-38.
Eckman, J. E. (1990). A model of passive settlement by planktonic larvae onto bottoms of differing roughness. *Limnol. Oceanogr.* **35**, 887-901.
Eckman, J. E., Werner, F. E. and Gross, T. F. (1994). Modelling some effects of behavior on larval settlement in a turbulent boundary layer. *Deep Sea Res. II Top. Stud. Oceanogr.* **41**, 185-208.
Ellis, I. and Kempf, S. C. (2011). Characterization of the central nervous system and various peripheral innervations during larval development of the oyster *Crassostrea virginica*. *Invertebr. Biol.* **130**, 236-250.
Fabry, V. J., Seibel, B. A., Feely, R. A. and Orr, J. C. (2008). Impacts of ocean acidification on marine fauna and ecosystem processes. *ICES J. Mar. Sci.* **65**, 414-432.
Fields, D. M. (2010). Orientation affects the sensitivity of *Acartia tonsa* to fluid mechanical signals. *Mar. Biol.* **157**, 505-514.
Fuchs, H. L. and Reidenbach, M. A. (2013). Biophysical constraints on optimal patch lengths for settlement of a reef-building bivalve. *PLoS ONE* **8**, e71506.
Fuchs, H. L., Mullineaux, L. S. and Solow, A. R. (2004). Sinking behavior of gastropod larvae (*Ilyanassa obsoleta*) in turbulence. *Limnol. Oceanogr.* **49**, 1937-1948.
Fuchs, H. L., Neubert, M. G. and Mullineaux, L. S. (2007). Effects of turbulence-mediated larval behavior on larval supply and settlement in tidal currents. *Limnol. Oceanogr.* **52**, 1156-1165.
Fuchs, H. L., Solow, A. R. and Mullineaux, L. S. (2010). Larval responses to turbulence and temperature in a tidal inlet: habitat selection by dispersing gastropods? *J. Mar. Res.* **68**, 153-188.
Fuchs, H. L., Hunter, E. J., Schmitt, E. L. and Guazzo, R. A. (2013). Active downward propulsion by oyster larvae in turbulence. *J. Exp. Biol.* **216**, 1458-1469.
Fuchs, H. L., Gerbi, G. P., Hunter, E. J., Christman, A. J. and Diez, F. J. (2015). Hydrodynamic sensing and behavior by oyster larvae in turbulence and waves. *J. Exp. Biol.* **218**, 1419-1432.
Gallager, S. M. (1993). Hydrodynamic disturbances produced by small zooplankton: case study for the veliger larva of a bivalve mollusc. *J. Plankton Res.* **15**, 1277-1296.
Gargett, A. E., Osborn, T. R. and Nasmyth, P. W. (1984). Local isotropy and the decay of turbulence in a stratified fluid. *J. Fluid Mech.* **144**, 231-280.
Gross, T. F., Werner, F. E. and Eckman, J. E. (1992). Numerical modeling of larval settlement in turbulent bottom boundary layers. *J. Mar. Res.* **50**, 611-642.
Grünbaum, D. and Strathmann, R. R. (2003). Form, performance and trade-offs in swimming and stability of armed larvae. *J. Mar. Res.* **61**, 659-691.
Guasto, J. S., Rusconi, R. and Stocker, R. (2012). Fluid mechanics of planktonic microorganisms. *Annu. Rev. Fluid Mech.* **44**, 373-400.
Hanlon, R. T., Bidwell, J. P. and Tait, R. (1989). Strontium is required for statolith development and thus normal swimming behaviour of hatchling cephalopods. *J. Exp. Biol.* **141**, 187-195.
Heuch, P. A. and Karlsen, E. (1997). Detection of infrasonic water oscillations by copepodids of *Lepeophtheirus salmonis* (Copepoda: Caligida). *J. Plankton Res.* **19**, 735-747.
Higham, T. E., Day, S. W. and Wainwright, P. C. (2006). Multidimensional analysis of suction feeding performance in fishes: fluid speed, acceleration, strike accuracy and the ingested volume of water. *J. Exp. Biol.* **209**, 2713-2725.
Holzman, R., Collar, D. C., Day, S. W., Bishop, K. L. and Wainwright, P. C. (2008). Scaling of suction-induced flows in bluegill: morphological and kinematic predictors for the ontogeny of feeding performance. *J. Exp. Biol.* **211**, 2658-2668.
Jackson, G. A. (1994). Particle trajectories in a rotating cylinder: implications for aggregation incubations. *Deep Sea Res. I Oceanogr. Res. Paper.* **41**, 429-437.
Jakobsen, H. H. (2001). Escape response of planktonic protists to fluid mechanical signals. *Mar. Ecol. Prog. Ser.* **214**, 67-78.
Jonsson, P. R., André, C. and Lindegarth, M. (1991). Swimming behaviour of marine bivalve larvae in a flume boundary-layer flow: evidence for near-bottom confinement. *Mar. Ecol. Prog. Ser.* **79**, 67-76.
Kaplan, M. B., Mooney, T. A., McCorkle, D. C. and Cohen, A. L. (2013). Adverse effects of ocean acidification on early development of squid (*Doryteuthis pealeii*). *PLoS ONE* **8**, e63714.
Karp-Boss, L. and Jumars, P. A. (1998). Motion of diatom chains in steady shear flow. *Limnol. Oceanogr.* **43**, 1767-1773.
Kennedy, V. S. and Sanford, L. P. (1999). Characteristics of relatively unexploited beds of the eastern oyster, *Crassostrea virginica*, and early restoration program. In *Oyster Reef Habitat Restoration: A Synopsis And Synthesis of Approaches* (ed. M. W. Luckenbach, R. Mann and J. A. Wesson), pp. 25-46. Williamsburg, VA: VIMS Press.
Kessler, J. O. (1986). The external dynamics of swimming micro-organisms. *Prog. Phycol. Res.* **4**, 257-291.
Khalitov, D. A. and Longmire, E. K. (2002). Simultaneous two-phase PIV by two-parameter phase discrimination. *Exp. Fluids* **32**, 252-268.

Kiger, K. T. and Pan, C. (2000). PIV technique for the simultaneous measurement of dilute two-phase flows. *J. Fluids Eng.* **122**, 811-818.
Kim, C.-K., Park, K., Powers, S. P., Graham, W. M. and Bayha, K. M. (2010). Oyster larval transport in coastal Alabama: dominance of physical transport over biological behavior in a shallow estuary. *J. Geophys. Res.* **115**, C10019.
Kiørboe, T. (2011). How zooplankton feed: mechanisms, traits and trade-offs. *Biol. Rev.* **86**, 311-339.
Kiørboe, T., Saiz, E. and Visser, A. (1999). Hydrodynamic signal perception in the copepod *Acartia tonsa*. *Mar. Ecol. Prog. Ser.* **179**, 97-111.
Knight-Jones, E. W. (1953). Laboratory experiments on gregariousness during setting in *Balanus balanoides* and other barnacles. *J. Exp. Biol.* **30**, 584-598.
Koehl, M. A. R., Crimaldi, J. P. and Dombroski, D. E. (2013). Wind chop and ship wakes determine hydrodynamic stresses on larvae settling on different microhabitats in fouling communities. *Mar. Ecol. Prog. Ser.* **479**, 47-62.
Latz, M. I., Case, J. F. and Gran, R. L. (1994). Excitation of bioluminescence by laminar fluid shear associated with simple Couette flow. *Limnol. Oceanogr.* **39**, 1424-1439.
Levi, R., Varona, P., Arshavsky, Y. I., Rabinovich, M. I. and Selverston, A. I. (2004). Dual sensory-motor function for a molluskan statocyst network. *J. Neurophysiol.* **91**, 336-345.
Lillis, A., Eggleston, D. B. and Bohnenstiehl, D. R. (2013). Oyster larvae settle in response to habitat-associated underwater sounds. *PLoS ONE* **8**, e79337.
Mackie, G. O., Singla, C. L. and Thiriot-Quievreux, C. (1976). Nervous control of ciliary activity in gastropod larvae. *Biol. Bull.* **151**, 182-199.
Marshall, D. J. and Keough, M. J. (2003). Variation in the dispersal potential of non-feeding invertebrate larvae: the desperate larva hypothesis and larval size. *Mar. Ecol. Prog. Ser.* **255**, 145-153.
Maxey, M. R. and Riley, J. J. (1983). Equation of motion for a small rigid sphere in a nonuniform flow. *Phys. Fluids* **26**, 883-889.
McDonald, K. A. (2012). Earliest ciliary swimming effects vertical transport of planktonic embryos in turbulence and shear flow. *J. Exp. Biol.* **215**, 141-151.
McNair, J. N., Newbold, J. D. and Hart, D. D. (1997). Turbulent transport of suspended particles and dispersing benthic organisms: how long to hit bottom? *J. Theor. Biol.* **188**, 29-52.
Mei, R., Adrian, R. J. and Hanratty, T. J. (1991). Particle dispersion in isotropic turbulence under Stokes drag and Basset force with gravitational settling. *J. Fluid Mech.* **225**, 481-495.
Miller, A. W., Reynolds, A. C., Sobrino, C. and Riedel, G. F. (2009). Shellfish face uncertain future in high CO_2 world: influence of acidification on oyster larvae calcification and growth in estuaries. *PLoS ONE* **4**, e5661.
Mogami, Y., Ishii, J. and Baba, S. A. (2001). Theoretical and experimental dissection of gravity-dependent mechanical orientation in gravitactic microorganisms. *Biol. Bull.* **201**, 26-33.
Mooney, T. A., Hanlon, R. T., Christensen-Dalsgaard, J., Madsen, P. T., Ketten, D. R. and Nachtigall, P. E. (2010). Sound detection by the longfin squid (*Loligo pealeii*) studied with auditory evoked potentials: sensitivity to low-frequency particle motion and not pressure. *J. Exp. Biol.* **213**, 3748-3759.
Mullineaux, L. S. and Garland, E. D. (1993). Larval recruitment in response to manipulated field flows. *Mar. Biol.* **116**, 667-683.
Naitoh, Y. and Eckert, R. (1969). Ionic mechanisms controlling behavioral responses of Paramecium to mechanical stimulation. *Science* **164**, 963-965.
North, E. W., Schlag, Z., Hood, R. R., Li, M., Zhong, L., Gross, T. and Kennedy, V. S. (2008). Vertical swimming behavior influences the dispersal of simulated oyster larvae in a coupled particle-tracking and hydrodynamic model of Chesapeake Bay. *Mar. Ecol. Prog. Ser.* **359**, 99-115.
Nowell, A. R. M. and Jumars, P. A. (1984). Flow environments of aquatic benthos. *Annu. Rev. Ecol. Syst.* **15**, 303-328.
Pennington, J. T. and Strathmann, R. R. (1990). Consequences of the calcite skeletons of planktonic echinoderm larvae for orientation, swimming, and shape. *Biol. Bull.* **179**, 121-133.
Prytherch, H. F. (1934). The role of copper in the setting, metamorphosis, and distribution of the American oyster, *Ostrea virginica*. *Ecol. Monogr.* **4**, 47-107.
Reidenbach, M. A., Koseff, J. R. and Koehl, M. A. R. (2009). Hydrodynamic forces on larvae affect their settlement on coral reefs in turbulent, wave-driven flow. *Limnol. Oceanogr.* **54**, 318-330.
Rubey, W. W. (1933). Settling velocity of gravel, sand, and silt particles. *Am. J. Sci.* **25**, 325-338.
Samson, J. E., Mooney, T. A., Gussekloo, S. W. S. and Hanlon, R. T. (2014). Graded behavioral responses and habituation to sound in the common cuttlefish *Sepia officinalis*. *J. Exp. Biol.* **217**, 4347-4355.
Shanks, A. L. (2009). Pelagic larval duration and dispersal distance revisited. *Biol. Bull.* **216**, 373-385.
Strathmann, R. R. and Grunbaum, D. (2006). Good eaters, poor swimmers: compromises in larval form. *Integr. Comp. Biol.* **46**, 312-322.
Strickler, J. R. and Bal, A. K. (1973). Setae of the first antennae of the copepod *Cyclops scutifer* (Sars): their structure and importance. *Proc. Natl. Acad. Sci. USA* **70**, 2656-2659.
Styles, R. (2015). Flow and turbulence over an oyster reef. *J. Coastal Res.* **31**, 978-985.
Tamburri, M. N., Zimmer-Faust, R. K. and Tamplin, M. L. (1992). Natural sources and properties of chemical inducers mediating settlement of oyster larvae: a re-examination. *Biol. Bull.* **183**, 327-338.
Taylor, G. I. (1923). Stability of a viscous liquid contained between two rotating cylinders. *Philos. Trans. R. Soc. A Math. Phys. Eng. Sci.* **223**, 289-343.
Taylor, G. I. (1936). Fluid friction between rotating cylinders. I. Torque measurements. *Proc. R. Soc. Ser. A Math. Phys. Eng. Sci.* **157**, 546-564.
Tennekes, H. and Lumley, J. L. (1972). *A First Course in Turbulence*. MIT Press: Cambridge, MA.
Tooby, P. F., Wick, G. L. and Isaacs, J. D. (1977). The motion of a small sphere in a rotating velocity field: a possible mechanism for suspending particles in turbulence. *J. Geophys. Res.* **82**, 2096-2100.
Turner, E. J., Zimmer-Faust, R. K., Palmer, M. A., Luckenbach, M. and Pentcheff, N. D. (1994). Settlement of oyster (*Crassostrea virginica*) larvae: effects of water flow and a water-soluble chemical cue. *Limnol. Oceanogr.* **39**, 1579-1593.
Wainwright, P., Carroll, A. M., Collar, D. C., Day, S. W., Higham, T. E. and Holzman, R. A. (2007). Suction feeding mechanics, performance, and diversity in fishes. *Integr. Comp. Biol.* **47**, 96-106.
Waldbusser, G. G., Voigt, E. P., Bergschneider, H., Green, M. A. and Newell, R. I. E. (2011). Biocalcification in the eastern oyster (*Crassostrea virginica*) in relation to long-term trends in Chesapeake Bay pH. *Estuaries Coasts* **34**, 221-231.
Wang, Z. A. and Cai, W.-J. (2004). Carbon dioxide degassing and inorganic carbon export from a marsh-dominated estuary (the Duplin River): a marsh CO_2 pump. *Limnol. Oceanogr.* **49**, 341-354.
Warnaars, T. A. and Hondzo, M. (2006). Small-scale fluid motion mediates growth and nutrient uptake of *Selenastrum capricornutum*. *Freshwater Biol.* **51**, 999-1015.
Webb, P. W. (2002). Control of posture, depth, and swimming trajectories of fishes. *Integr. Comp. Biol.* **42**, 94-101.
Welch, J. M. and Forward, R. B., Jr. (2001). Flood tide transport of blue crab, *Callinectes sapidus*, postlarvae: behavioral responses to salinity and turbulence. *Mar. Biol.* **139**, 911-918.
Wereley, S. T. and Lueptow, R. M. (1999). Velocity field for Taylor-Couette flow with an axial flow. *Phys. Fluids* **11**, 3637-3649.
Whitman, E. R. and Reidenbach, M. A. (2012). Benthic flow environments affect recruitment of Crassostrea virginica larvae to an intertidal oyster reef. *Mar. Ecol. Prog. Ser.* **463**, 177-191.
Yen, J., Lenz, P. H., Gassie, D. V. and Hartline, D. K. (1992). Mechanoreception in marine copepods: electrophysiological studies on the first antennae. *J. Plankton Res.* **14**, 495-512.
Young, C. M. (1995). Behavior and locomotion during the dispersal phase of larval life. In *Ecology of Marine Invertebrate Larvae* (ed. L. McEdward), pp. 249-278. CRC Press: Boca Raton, FL.
Zacherl, D. C., Manríquez, P. H., Paradis, G., Day, R. W., Castilla, J. C., Warner, R. R., Lea, D. W. and Gaines, S. D. (2003). Trace elemental fingerprinting of gastropod statoliths to study larval dispersal trajectories. *Mar. Ecol. Prog. Ser.* **248**, 297-303.